The International Journal of Advanced Manufacturing Technology (2018) 98:1591–1604
https://doi.org/10.1007/s00170-018-2186-4

ORIGINAL ARTICLE

Electromechanical integrated modeling and analysis for the direct-driven feed system in machine tools

Xiaojun Yang [1,2] · Dun Lu [1,2] · Hui Liu [1,2] · Wanhua Zhao [1,2]

Received: 24 November 2017 / Accepted: 13 May 2018 / Published online: 21 June 2018

Abstract

The permanent magnet linear synchronous motor (PMLSM) feed system realizes the direct drive. All the intermediate mechanical transmission parts are canceled and then the motor mover is directly connected with the driven components. The interaction between servo system and mechanical system becomes more close and complex, affecting the dynamic performance of the direct-driven feed system. In this paper, the dynamic characteristics of the drive circuit, PMLSM, control loops, and mechanical system are analyzed, and then an electromechanical integrated modeling method for the direct-driven feed system is proposed. Firstly, the dynamic precision of the feed system and electromechanical analytical model is studied. Then the nonlinearities of the drive circuit and PMLSM are researched. The analytical expression of the motor thrust is derived. What is more, the mechanical dynamic model is set up using the Lagrange equation and the main forms of the vibrations are discussed. Finally, the electromechanical integrated model is established and the experiments are carried out to verify the theoretical results. The results show that the proposed integrated modeling method can accurately represent the dynamic precision of the direct-driven feed system, which can provide the theoretical foundation for analyzing the electromechanical couplings and compensation methods.

Keywords Direct-driven feed system · Electromechanical integrated model · Servo system · Mechanical system · Dynamic precision

Nomenclature

$x_a(t)$	The actual displacement/mm
v	Speed of the mover/m/min
H_A	The height of mover/mm
g	The thickness of air gap/mm
w_s	The tooth pitch/mm
i_{ref}	The current command/A
io	The output of current loop/A
τ	Pole pitch/mm
B_{nx}	The electromagnetic coefficients in the tangential direction
x_o	The position output/mm
k_{iy}	The stiffness of ith block in y direction/N/m, i = 1, 2, 3, 4, 5, 6
c_{iy}	The damping of ith block in y direction, i = 1, 2, 3, 4, 5, 6
K_s	Servo stiffness
t_{on}	The opening time/ms
T_d	The dead time/ms
V_{dc}	The power voltage/V
u_{as}	The voltage harmonics of a phase winding caused by the PWM/V
M	The modulation ratio
ω_c	The frequency of the reference wave/Hz
E_{ma}	The harmonics of the back electromotive force without load
l	The width of the coil/mm
B_r	The remanence of the permanent magnet

Highlights
1. The electromechanical analytical model of the direct-driven feed system is put forward.
2. The nonlinearity of servo circuit, current loop, and linear motor is researched.
3. An electromechanical integrated modeling method for the direct-driven feed system is proposed.
4. The integrated model is verified by transient error, following error, and displacement fluctuation.

✉ Wanhua Zhao
whzhao@mail.xjtu.edu.cn

[1] School of Mechanical Engineering, Xi'an Jiaotong University, Room A315 of North Side, The West No.5 Building, Qujiang Campus, No.99, Yanxiang Road, Xi'an 710049, Shaanxi, China

[2] State Key Laboratory for Manufacturing Systems Engineering, Xi'an Jiaotong University, Xi'an 710054, China

T_{pwm} The time of the inverter/ms
T_i The integral time of the current controller/ms
K_a The feedback gain
R_a The resistance of the motor coil
T_a The electrical time of the linear motor, and $T_a = L_a/R_a$
M_{ab} The mutual inductance between a phase and b phase
i_k The armature current, $k = a, b, c$
E_{mk} The back electromotive forces without load, $k = a, b, c$
g_e The equivalent air gap coefficient
ε The asymmetric inductance coefficient
I_m The amplitude of the m-order current harmonic
m The total mass of drive components
J_x The rotational inertia of mechanical system around x-axis/kgm^2
a The length of the worktable/mm
b The width of the worktable/mm
a_1 The length of the motor mover/mm
c_1 The height of the motor mover/mm
K_n The Hertz contact coefficient
Q_p The preload/N
F_n The normal counterforce of F/N
K_y The tangential contact stiffness of single block
K_z The normal contact stiffness of single block
β_c Rayleigh damping coefficient
$k_{\theta y}$ The stiffness of pitch
K_p Proportional gain of position controller
T_v Integral time constant of speed controller
K_F Force constant/N/A
x_e The displacement signal of the reading head in feed direction/mm
h_m The vertical distance between the center of mover and coordinate origin/mm
L_2 The distance between two blocks on the same guide rail/mm
δ_d The dynamic precision/mm
$x_c(t)$ The command displacement/mm
L The length of mover/mm
h_s The height of winding/mm
τ_s The pitch/mm
h The thickness of permanent magnet/mm
w_p The width of permanent magnet/mm
g The thickness of air gap
x_i The position command/mm
B_{ny} The electromagnetic coefficients in the normal direction
F_r The disturbance/N
k_{iz} The stiffness of ith block in z direction/N/m, $i = 1, 2, 3, 4, 5, 6$
c_{iz} The damping of ith block in z direction, $i = 1, 2, 3, 4, 5, 6$
c_{ix} The damping of ith block in x direction, $i = 1, 2, 3, 4, 5, 6$
t_{off} The closing time/ms
T_s The working period time/ms
u_{ao} The voltage harmonics of a phase winding caused by the dead-zone effect/V
E The DC voltage/V
ω_0 The frequency modulation wave/Hz
J_n The Bessel function
N The coil turns
v_a The speed of mover/m/min
K_{pwm} The gain of the inverter
K_i The gain of the current controller/ms
T_{if} The time of the filter/ms
L_a The inductance of the motor coil
K_F The thrust constant
L_a The self-inductance of a phase winding
M_{ac} The mutual inductance between a phase and c phase
E_{lk} The back electromotive forces with load, $k = a, b, c$
λ_0 The permeability, and $\lambda_0 = \mu_0/g_e$
X_L The distance away from the mover end
L_{a0} The amplitude of the inductance
m_w The mass of the worktable/kg
m_m The mass of the mover/kg
J_y The rotational inertia of mechanical system around y-axis/kgm^2
J_z The rotational inertia of mechanical system around z-axis/kgm^2
c The height of the worktable/mm
b_1 The width of the motor mover/mm
δ_n Normal deformation/μm
Q_n The normal load/N
F The external load/N
α The contact angle
α_c Rayleigh damping coefficient
$c_{\theta y}$ The damping of pitch
T_p The equivalent disturbance torque
K_v Proportional gain of speed controller
K_A Proportional gain of the current controller
x_w The displacement of the worktable in feed direction/mm
f The friction/N
h_b The vertical distance between the center of block and coordinate origin/mm
L_1 The distance between two guide rails/mm
K_s The servo stiffness

1 Introduction

Comparing with the traditional ball screw feed system, the permanent magnet linear synchronous motor (PMLSM) feed system realizes the direct drive and then has plenty of advantages, such as simple structure, large thrust, good characteristics, high speed, and high precision. The direct-driven feed

system has a broad application prospect in the high-speed and high-precision machining [1, 2].

With the deepening of the research, the thrust fluctuations and disturbance susceptibility become the most prominent problems for the direct-driven feed system. The thrust harmonics produced by the nonlinearities of the driven circuit and motor structure have obtained the attentions of many scholars. A great many of the structural optimization methods are put forward [3–10]. The amplitudes of thrust harmonics become less than 5% of the nominal thrust. However, because the motor mover is connected with the driven components, the thrust harmonics with low amplitudes directly act on the mechanical system, leading to non-negligible displacement fluctuations [11, 12]. There is also much research focused on the compensation methods to improve the dynamic precision [13–21]. The above studies have important significance to improve the dynamic performance of the direct-driven feed system. However, at present, the ball screw feed system with a large lead screw is still widely used in the machine tools, especially high-speed and high-precision machine tools. In addition to the high cost of the PMLSM itself, the electromechanical couplings and mechanical vibrations in the motion process are the major problems, which restrict the popularization and application of the direct-driven feed system.

In the present research, the servo system and mechanical system are separated artificially. The analyses about the thrust only aim at PMLSM, which does not map to the final displacement fluctuation. Meanwhile, in the control model, the mechanical system is just equivalent to a simple single moment of inertia of the system. However, in fact, the thrust harmonics and other disturbances directly act on the mechanical system, leading to obvious mechanical vibrations with multi-modes. Meanwhile, the mechanical dynamic characteristics also have important effects on the thrust characteristics. The interaction between the servo system and mechanical system becomes more close and complex due to zero transmission structure. Kim et al. [22] proposed an integrated design methodology for the ball screw-driven servomechanisms. Im et al. [23] analyzed the dynamic behaviors of a BLDC motor considering the mechanical and electromagnetic interaction due to the air gap variation. Neugebauer et al. [24] presented the integration of mechatronics modules to the machine tools and discussed the effects of their interaction on the reliability of the machine tools. Weck et al. [25] analyzed the effects of the encoder's vibrations on the bandwidth of the current loop and control parameters for the linear motor feed system. Most of the current studies focused on the traditional feed system. There is little research about the electromechanical interaction in direct-driven feed system. It is important and necessary to set up the electromechanical integrated model for the direct-driven feed system, which can be used to analyze the effects of different disturbances, the electromechanical couplings, integrated design, and compensation methods.

Therefore, in this paper, oriented to the dynamic precision of the direct-driven feed system, the electromechanical integrated model is established considering the characteristics of the servo drive circuit, PMLSM, and mechanical system. In the second section, the electromechanical analytical model is put forward based on the analysis of the structure and error sources of the feed system. In the third section, the nonlinearity of the drive circuit is studied and the servo current harmonics are calculated. What is more, the nonlinearity of the PMLSM itself is analyzed and the analytical expression of motor thrust is derived. In the fourth section, the mechanical dynamic model is set up using the Lagrange equation and the main forms of the vibrations are discussed. Finally, the electromechanical integrated model is established and the experiments are carried out in the last two sections.

2 Electromechanical analytical model of the direct-driven feed system

The direct-driven feed system is consisted of numerical control (NC) system, proportional–integral–derivative (PID) controller, drive circuit, PMLSM, mechanical components, linear encoder, and other supporting components. The PMLSM has two parts: mover and stator. The stator is a permanent magnet installed on the magnetic steel. The motor mover is directly connected with the drive components. The drive circuit is used to amplify the weak voltage signal to drive PMLSM. The PID controller, which is consisted of position loop, velocity loop, and current loop, determines the performance of the servo system. The high-precision linear encoder collects the real-time displacement signal to form the feedback loop. The characteristic of the NC system is not discussed here.

In order to comprehensively describe the precision of the direct-driven feed system in motion process with high speed, the deviation between the actual trajectory and the ideal NC command is defined as the dynamic precision [26], that is

$$\delta_d(t) = x_a(t) - x_c(t) \tag{1}$$

In accordance with the different motion processes of the feed system, the dynamic precision can be divided into three indexes which are transient error, steady-state following error, and displacement fluctuation as shown in Fig. 1. The transient error represents errors produced by the abrupt change of the command, mechanical clearance, and nonlinear friction in the process of start and stop. The following error represents the steady-state deviation between the actual trajectory and the command considering the acceleration process and system delay. The displacement fluctuation represents the mechanical vibrations due to the thrust harmonics and outside disturbances in the steady-state motion process.

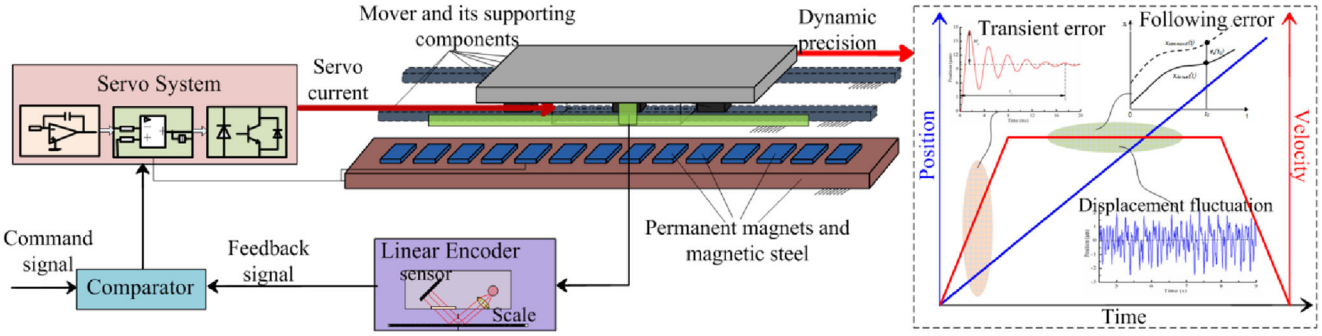

Fig. 1 The structure and dynamic precision of the direct-driven feed system

Based on the experimental tests, the author team found that the dynamic precision of the direct-driven feed system depends on the characteristics of the servo system, the mechanical system, and their interaction. Due to the manufacturing errors and characteristics of electronic devices, the drive circuit has various nonlinear factors, such as dead-zone effect, modulation harmonics, and electromotive force harmonics. Meanwhile, the magnetic field of permanent magnet also has many harmonics due to the structural nonlinearity of the motor itself, such as end effect, slot effect, and magnetic linkage harmonics. The above nonlinear factors will produce lots of thrust harmonics which directly act on the mechanical system, leading to displacement fluctuations. What is more, the mechanical system is not an ideal single moment of inertia of the system. Under the motivation of the thrust harmonics and other disturbances, different kinds of the vibrations may occur, which will affect the motor thrust through the zero transmission structure and full-close-loop feedback system. According to the working principle of each component and considering the main sources of disturbance errors, the electromechanical analytical model is established as shown in Fig. 2.

In Fig. 2, there are five sub-models, which are model of the drive circuit, control model of the current loop, analytical model of the linear motor, mechanical dynamic model, and integrate model.

3 Analysis of the characteristics of the servo system

3.1 The characteristics of drive circuit

The drive circuit includes rectifier circuit, filter circuit, inverter circuit, modulation circuit, motor coil, and other auxiliary circuit, which is shown in Fig. 3.

In order to produce the ideal thrust force, the three phase currents are needed to be ideal sine waveforms. However, in

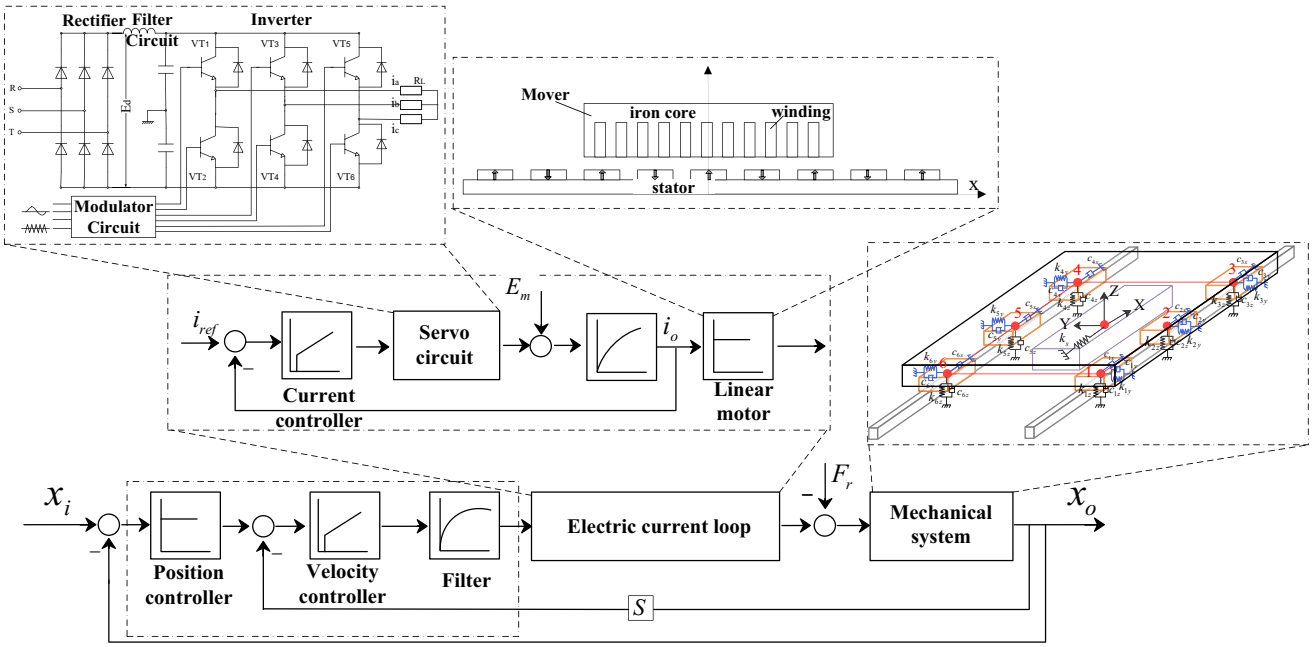

Fig. 2 Electromechanical analytical model of the direct-driven feed system

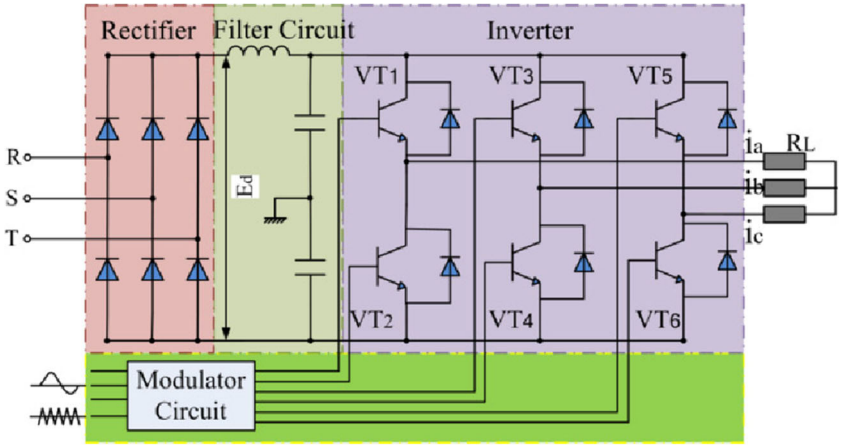

Fig. 3 The structure of the servo drive circuit

practice, there are different kinds of the nonlinear factors in the drive circuit, leading to lots of current harmonics. Taking a phase coil as the example, the main harmonics are calculated as follows.

The voltage harmonics caused by the dead-zone effect in the inverter is equal to [27]

$$u_{ao} = \sum_{k=1,5,7\cdots}^{\infty} u_{ka} \sin k\omega t \tag{2}$$

where $u_{ka} = \frac{8\Delta V}{3k\pi} \times \left(1 + \sin\frac{k\pi}{2}\sin\frac{k\pi}{6}\right), k = 1,5,7\cdots; \Delta V = t_{off} - t_{on} - T\frac{d}{2T_s V_{dc}}$.

The voltage harmonics with high frequencies produced by pulse width modulation (PWM) can be obtained as [28, 29]:

$$u_{as} = \frac{8}{3}\sum_{n=3,5,7,\ldots\ldots}^{\infty} \frac{E}{\pi}\frac{1}{n\frac{\omega_0}{\omega_c}} J_n\left(n\frac{\omega_0}{\omega_c}\frac{M\pi}{2}\right)\sin\frac{n\pi}{2}\cdot\cos\left[\frac{n\pi}{2}\left(1+\frac{\omega_0}{\omega_c}\right)\right]\sin^2\frac{n\pi}{3}\sin\left(n\omega_0 t + \frac{\pi}{4}\right) \tag{3}$$

The harmonics of the back electromotive force (Emf) without load can be given by [30]:

$$E_{ma} = \sum_{n=1,3,5,\ldots} \frac{8Nlv_a B_r}{\pi}\frac{1}{n}\sin\frac{n\pi w_p}{2\tau} \times \frac{\sinh\left(\frac{n\pi}{\tau}h\right)}{\sinh\left[\frac{n\pi}{\tau}(h+g)\right]}\sin\left(\frac{n\pi v_a t}{\tau}\right) \tag{4}$$

Finally, the voltage harmonics acted on the motor coil of a phase can be obtained as:

$$u_{ra} = u_{ao} + u_{as} - E_{ma} \tag{5}$$

3.2 The characteristics of current loop

The current loop, which is the inner loop and can restrict the peak current and acceleration of the current response, has important effect on the dynamic characteristics of the feed system. The current loop is composed of filters, control regulator, PWM inverter, motor coil, feedback system, and other detection device, as shown in Fig. 4.

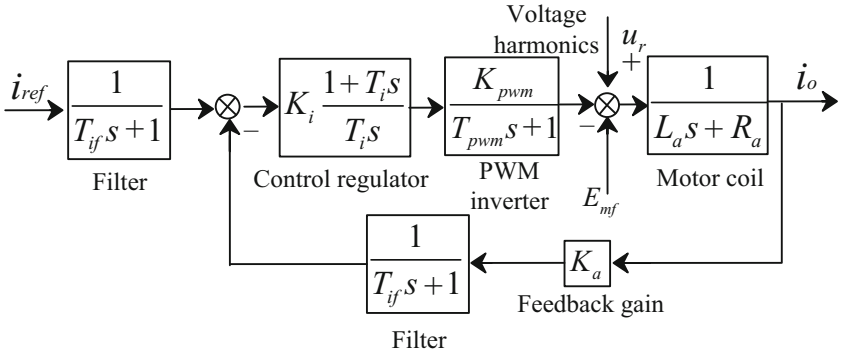

Fig. 4 The control structure of current loop

The filter and inverter are merged into an inertial unit because their time constants are much smaller than the electrical time of the PMLSM. The gain of feedback loop is assumed to be unit. Meanwhile, the filter in the feedback loop is neglected. The voltage harmonics caused by the inverter, PWM, and Emf are taken as the external disturbances and introduced into the current loop. The model in Fig. 4 can be simplified as shown in Fig. 5.

The transfer function can be obtained through Fig. 5 as:

$$i_0 = \frac{K_i K_{pwm}(T_i s+1)/R_a}{T_i s\left[(T_{if}+T_{pwm})s+1\right](T_a s+1)+K_i K_{pwm}(T_i s+1)/R_a} i_{ref} + \frac{T_i s\left[(T_{if}+T_{pwm})s+1\right]/R_a}{T_i s\left[(T_{if}+T_{pwm})s+1\right](T_a s+1)+K_i K_{pwm}(T_i s+1)/R_a} u_r \quad (6)$$

It can be obtained from Eq. (6) that the output of the current loop has two parts, which are outputs due to current command and voltage disturbances.

Assuming the current command is $i_{ref}(t) = I_0 \sin\omega_I t$, its Laplace form is $i_{ref}(s) = \frac{I_0\omega_I}{s^2+\omega_I^2}$.

Assuming one of the voltage disturbance is $u_r(t) = U_r \sin\omega_u t$, its Laplace form is $u_r(s) = \frac{U_r\omega_u}{s^2+\omega_u^2}$.

The final output of the current loop can be given by

$$i(t) = \frac{K_i K_{pwm}}{T_i(T_{if}+T_{pwm})R\omega_0}\left(Ae^{-at}\cos\omega_0 t + \frac{B-Aa}{\omega_0}e^{-at}\sin\omega_0 t\right) + A' e^{-s_1 t} + B' e^{-s_2 t} + C' e^{-s_3 t} + \frac{K_i K_{pwm}}{T_i(T_{if}+T_{pwm})R\omega_0}\left(C\cos\omega t + \frac{D}{\omega}\sin\omega t\right) + D'\cos\omega_r t + \frac{E'}{\omega_r}\sin\omega_r t \quad (7)$$

where

$$A = \frac{2a\omega_0\omega_I I_0}{\left(a^2+\omega_0^2-\omega_I^2\right)^2+4a^2\omega_I^2}; B = \frac{\left(3a^2-\omega_0^2+\omega_I^2\right)\omega_0\omega_I I_0}{\left(a^2+\omega_0^2-\omega_I^2\right)^2+4a^2\omega_I^2};$$

$$C = \frac{-2a\omega_0\omega_I I_0}{\left(a^2+\omega_0^2-\omega_I^2\right)^2+4a^2\omega_I^2}; D = \frac{\left(a^2+\omega_0^2-\omega_I^2\right)\omega_0\omega_I I_0}{\left(a^2+\omega_0^2-\omega_I^2\right)^2+4a^2\omega_I^2};$$

$$E' = \frac{U_r\omega_u^3}{L\left(T_{if}+T_{pwm}\right)} \frac{\left(s_1s_2+s_2s_3+s_3s_1-\omega_u^2\right)+\left(T_{if}+T_{pwm}\right)\left[(s_1+s_2+s_3)\omega_u^2-s_1s_2s_3\right]}{\left[(s_1+s_2+s_3)\omega_u^2-s_1s_2s_3\right]^2+\omega_u^2\left(s_1s_2+s_2s_3+s_3s_1-\omega_u^2\right)^2}$$

$$D' = \frac{U_r\omega_u}{L\left(T_{if}+T_{pwm}\right)} \frac{\left(s_1s_2+s_2s_3+s_3s_1-\omega_u^2\right)\left(T_{if}+T_{pwm}\right)\omega_u^2-\left[(s_1+s_2+s_3)\omega_u^2-s_1s_2s_3\right]}{\left[(s_1+s_2+s_3)\omega_u^2-s_1s_2s_3\right]^2+\omega_u^2\left(s_1s_2+s_2s_3+s_3s_1-\omega_u^2\right)^2}$$

$$C' = B' = \frac{s_1D+E}{2s_1-s_2-s_3}, A' = -B'-C'-D', a = \frac{1}{2\left(T_{if}+T_{pwm}\right)}, \omega_0 = \sqrt{\frac{4K_iK_{pwm}K_a\left(T_{if}+T_{pwm}\right)-T_iR_a}{4\left(T_{if}+T_{pwm}\right)^2T_iR_a}}$$

s_1, s_2, and s_3 are the roots of the equation $T_i s[(T_{if}+T_{pwm})s+1](T_a s+1)+K_iK_{pwm}(T_i s+1)/R_a = 0$.

Ignoring the transient response, the current after the adjustment of the controller is shown as:

$$\begin{cases} i_a(t) = \sum_n I_{man}\sin[n(\omega t+\theta)] \\ i_b(t) = \sum_n I_{mbn}\sin[n(\omega t+\theta-2\pi/3)] n = 1,5,7,\ldots,6i\pm1 \\ i_c(t) = \sum_n I_{mcn}\sin[n(\omega t+\theta-4\pi/3)] \end{cases} \quad (8)$$

3.3 The characteristics of the PMLSM

The thrust is produced by the interaction between the traveling magnetic field caused by the primary current and the magnetic field caused by the permanent magnet. In addition to the current harmonics, the magnetic field of permanent magnet also has plenty of harmonics due to the structural nonlinearity of the PMLSM itself, such as end effect, slot effect, and magnetic linkage harmonics.

The analytical model of the magnetic field for PMLSM is established as shown in Fig. 6.

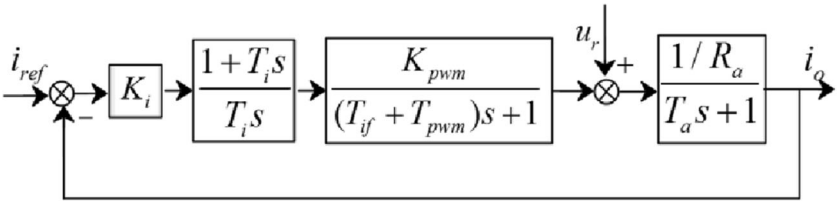

Fig. 5 The simplified structure of the current loop

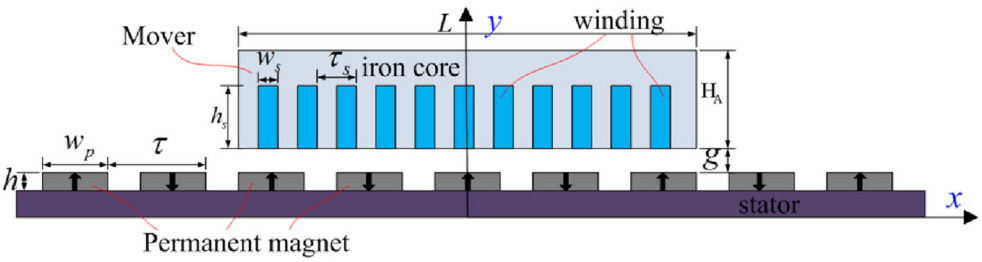

Fig. 6 The analytical model of the magnetic field for the PMLSM

According to Maxwell's equations, the magnetic field strength produced by the permanent magnet in the air gap area can be given by

$$\begin{cases} B_x(x) = \sum_{n=1,3,5\ldots}^{\infty} B_{nx}\sin\left(\frac{n\pi}{\tau}x\right) \\ B_y(x) = \sum_{n=1,3,5\ldots}^{\infty} B_{ny}\cos\left(\frac{n\pi}{\tau}x\right) \end{cases} \tag{9}$$

Because the tangential component of the magnetic field is much less than the normal one, only the B_y is considered here.

$$B(x) = \sum_{n=1,3,5\ldots}^{\infty} \frac{4B_r}{\pi}\frac{1}{n}\sin\frac{n\pi w_p}{2\tau} \times \frac{\sinh\left(\frac{n\pi}{\tau}h\right)}{\sinh\left[\frac{n\pi}{\tau}(h+g)\right]}\cos\left(\frac{n\pi}{\tau}x\right) \tag{10}$$

Using the conformal transformation method, the relative permeance functions considering the slot effect can be obtained as [8]:

$$\lambda_s(x) = a_0 + \sum_{n=1}^{\infty} a_n\cos\left(\frac{2n\pi}{\tau_s}x\right) \tag{11}$$

where $a_0 = 1-1.6\frac{w_s}{\tau_s}\beta(y)$, $a_n = -\frac{4}{n\pi}\beta(y)\left[0.5+\frac{\left(\frac{w_s}{\tau_s}n\right)^2}{0.78215-2\left(\frac{w_s}{\tau_s}n\right)^2}\right]\sin\left(1.6\pi\frac{w_s}{\tau_s}n\right)$

$$\beta(y) = \frac{1}{2}\left[1-\frac{1}{\sqrt{1+\left(\frac{w_s}{2K_e g}\right)^2(1+v^2)}}\right],\quad K_e = 1+\frac{h}{\mu_r\cdot g}.$$

Using the conformal transformation method, the relative permeance functions considering the end effect can be obtained as:

$$\lambda_e(x) = \begin{cases} e^{\frac{(x+L/2)}{2g'}} & x < -L/2 \\ 1 & -L/2 < x < L/2 \\ e^{\frac{(x-L/2)}{2g'}} & x > L/2 \end{cases} \tag{12}$$

where $g' = g + \frac{h}{\mu_r}$.

Finally, the magnetic field model in the air gap considering the slot effect and end effect can be given by:

$$B'(x) = \lambda_s(x)\cdot\lambda_e(x)\cdot B_y(x) = \lambda_s(vt)\cdot\lambda_e(vt)\cdot B(vt) \tag{13}$$

3.4 The characteristics of thrust harmonics

Using the energy method, the motor thrust can be calculated as:

$$F = \frac{1}{v}\left\{\frac{\partial}{\partial t}[(L_a+M_{ab}+M_{ac})\cdot i_a(t)] - Nl\frac{\partial}{\partial t}\left[\int_{x_a+\tau/2}^{x_a-\tau/2}B_a(x)dx\right]\right\}\cdot i_a + \frac{1}{v}\left\{\frac{\partial}{\partial t}[(L_b+M_{ab}+M_{bc})\cdot i_b(t)] - Nl\frac{\partial}{\partial t}\left[\int_{x_a+\tau/2}^{x_a-\tau/2}B_b(x)dx\right]\right\}\cdot i_b + \frac{1}{v}\left\{\frac{\partial}{\partial t}[(L_c+M_{bc}+M_{ac})\cdot i_c(t)] - Nl\frac{\partial}{\partial t}\left[\int_{x_a+\tau/2}^{x_a-\tau/2}B_c(x)dx\right]\right\}\cdot i_c \tag{14}$$

Substituting Eq. (8) and Eq. (13) into Eq. (14), the thrust can be obtained as follows.

$$F = F_0 + 3Nla_0\sum_i F_{6i}\sin\left(\frac{6i\pi v}{\tau}t\right) + \frac{3}{2}Nl\sum_i B_i a_i\cos\left(\frac{i\tau\pi}{\tau_s}\right)\cdot\sin\left(\frac{2iv\pi}{\tau_s}t\right) + \frac{3}{2}Nl\sum_i F_{6i}a_i\cdot\sin\left(\frac{6i\pi v}{\tau}t+\frac{2iv\pi}{\tau_s}t\right) + \frac{3}{2}Nl\sum_i F_{6i}a_i\cdot\sin\left(\frac{6i\pi v}{\tau}t-\frac{2iv\pi}{\tau_s}t\right) + \frac{w\lambda_0^2}{\mu_0}e^{\frac{(x_L+L/2)}{g_e}}\sum_n^{\infty}A_n^2\frac{\tau}{2n\pi}\sinh\left(\frac{2n\pi}{\tau}H_A\right)\cdot\cos\left[\frac{2n\pi}{\tau}\left(vt+\frac{n\tau-L}{2}\right)\right] + \frac{\varepsilon L_{a0}\pi}{\tau}\sum_{m=1,5,7\ldots}I_m^2\sin\frac{2m\pi}{\tau}vt \tag{15}$$

where $n = 1, 2, 3\ldots$, $i = 1, 2, 3\ldots$, B_n, and a_0, a_n, A_n are electromagnetic coefficients.

4 Analysis of the dynamic characteristics of the mechanical system

The mechanical system consists of the worktable, motor mover, linear guide, block, linear encoder, permanent magnet, and machine bed, which is shown in Fig. 7. Although the mechanical structure is much simpler than the traditional ball screw feed system, the direct-driven feed system still has complex mechanical characteristics considering the effects of the joints between the guide and blocks.

The center of the mass of the mover and the worktable is taken as the origin of coordinate. The mechanical dynamic model of the direct-driven feed system is established as shown in Fig. 8 using the lumped-mass method. Because the vertical magnetic force between the mover and stator is usually large (about 20 kN), every guide has three blocks. The flexibility of

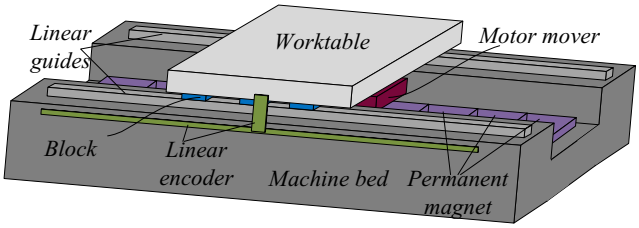

Fig. 7 The mechanical structure of the direct-driven feed system

the worktable and machine bed can be ignored. Comparing with the worktable and motor mover, the mass and geometric dimension of the block are very small, which are ignored here. The masses mainly include the mass of the worktable m_w and the mass of the motor mover m_m. The stiffness in the feed direction is equivalent to the servo stiffness K_s because there are not intermediate mechanical transmission components. K_s acts on the center of the mass of the mover and the worktable. The detail calculation of servo stiffness and contact stiffness is shown in [31]. The contact stiffness between the guide and each block is equivalent to the linear spring units (k_{iy}, k_{iz}, $i = 1, 2, 3, 4, 5, 6.$) which act on the center of the mass of each block in the directions of Y and Z. Ignoring the difference among blocks, $k_{iy} = K_y$, and $k_{iz} = K_z$. K_y and K_z are the tangential and normal stiffness of single block. The damping of the system is expressed as Rayleigh proportional damping of mass and stiffness. The motor thrust is acted on the center of the mass of the motor mover.

In the coordinate as shown in Fig. 9, the linear displacements and rotational vibrations are assumed as x, y, z, θ_x, θ_y, and θ_z. Using the Lagrange's equation, the mechanical model can be established as

$$\mathbf{M}\ddot{\mathbf{X}} + \mathbf{C}\dot{\mathbf{X}} + \mathbf{K}\mathbf{X} = \mathbf{F} \tag{16}$$

where,

$$\mathbf{M} = \begin{bmatrix} m & 0 & 0 & 0 & 0 & 0 \\ 0 & m & 0 & 0 & 0 & 0 \\ 0 & 0 & m & 0 & 0 & 0 \\ 0 & 0 & 0 & J_x & 0 & 0 \\ 0 & 0 & 0 & 0 & J_y & 0 \\ 0 & 0 & 0 & 0 & 0 & J_z \end{bmatrix},$$

$$\mathbf{K} = \begin{bmatrix} K_s & 0 & 0 & 0 & -K_s h_m & 0 \\ 0 & 6K_y & 0 & 6K_y h_b & 0 & 0 \\ 0 & 0 & 6K_z & 0 & 0 & 0 \\ 0 & 6K_y h_b & 0 & 6K_y h_b^2 + 1.5K_z L_1^2 & 0 & 0 \\ -K_s h_m & 0 & 0 & 0 & K_s h_m^2 + 4K_z L_2^2 & 0 \\ 0 & 0 & 0 & 0 & 0 & 4K_y L_2^2 \end{bmatrix}$$

$$\mathbf{C} = \alpha_c \mathbf{M} + \beta_c \mathbf{K}$$

Based on the analysis in [31], the coupled terms, which are the coupling between the pitch and vibration in x direction and the coupling between the roll and vibration in y direction, can be neglected. Therefore, Eq. (16) is simplified as

$$\mathbf{M}'\ddot{\mathbf{X}} + \mathbf{C}'\dot{\mathbf{X}} + \mathbf{K}'\mathbf{X} = \mathbf{F} \tag{17}$$

where,

$$\mathbf{M}' = \begin{bmatrix} m & 0 & 0 & 0 & 0 & 0 \\ 0 & m & 0 & 0 & 0 & 0 \\ 0 & 0 & m & 0 & 0 & 0 \\ 0 & 0 & 0 & J_x & 0 & 0 \\ 0 & 0 & 0 & 0 & J_y & 0 \\ 0 & 0 & 0 & 0 & 0 & J_z \end{bmatrix}$$

$$\mathbf{K}' = \begin{bmatrix} K_s & 0 & 0 & 0 & 0 & 0 \\ 0 & 6K_y & 0 & 0 & 0 & 0 \\ 0 & 0 & 6K_z & 0 & 0 & 0 \\ 0 & 0 & 0 & 6K_y h_b^2 + 1.5K_z L_1^2 & 0 & 0 \\ 0 & 0 & 0 & 0 & K_s h_m^2 + 4K_z L_2^2 & 0 \\ 0 & 0 & 0 & 0 & 0 & 4K_y L_2^2 \end{bmatrix}$$

$$\mathbf{C}' = \alpha_c \mathbf{M}' + \beta_c \mathbf{K}'$$

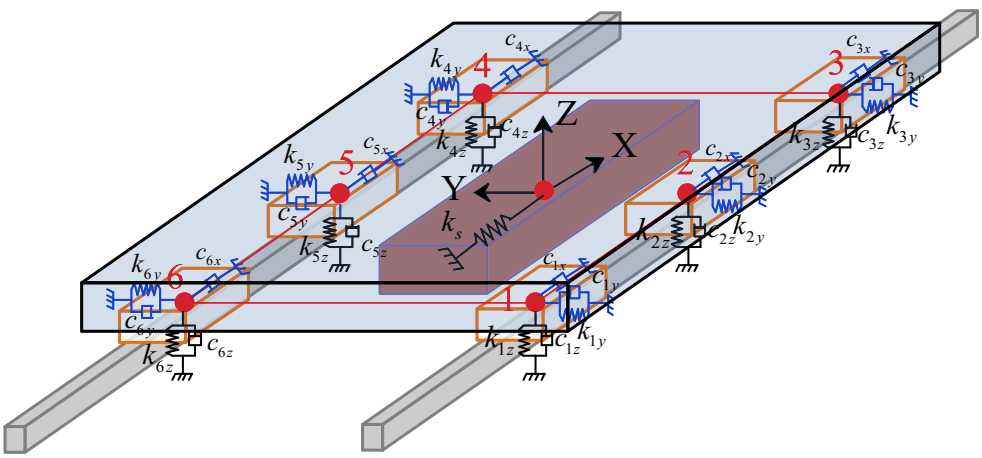

Fig. 8 The mechanical dynamic model of the direct-driven feed system

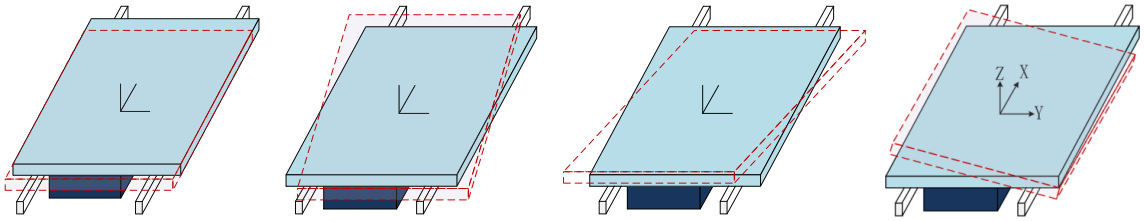

Fig. 9 The main mechanical vibrations in the direct-driven feed system. **a** Feed vibration. **b** Pitch vibration. **c** Yaw vibration. **d** Roll vibration

Because the stiffness and damping of the joints between the guide and block along the *Y* and *Z* directions are large, their vibrations can be ignored. Therefore, in this paper, only the mechanical vibration in the feed direction and rotational vibrations are considered as shown in Fig. 9.

In the fact, there are two kinds of the disturbances which are motor thrust harmonics and outside disturbance. Considering the difference between the displacement of the worktable and that of the linear encoder, the relationship between the output and input of the mechanical system can be obtained as follows.

$$\begin{bmatrix} x_w \\ \theta_p \\ \theta_r \\ \theta_y \end{bmatrix} = \begin{bmatrix} H_{mf} & H_{of} \\ H_{mp} & H_{op} \\ H_{mr} & H_{or} \\ H_{my} & H_{oy} \end{bmatrix} \times \begin{bmatrix} F_{\text{motor}} \\ F_{\text{out}} \end{bmatrix} \tag{18}$$

$$\begin{bmatrix} x_w \\ x_e \end{bmatrix} = \begin{bmatrix} H_{pf} & H_{rf} & H_{yf} \\ H_{pe} & H_{re} & H_{ye} \end{bmatrix} \times \begin{bmatrix} \theta_p \\ \theta_r \\ \theta_y \end{bmatrix} \tag{19}$$

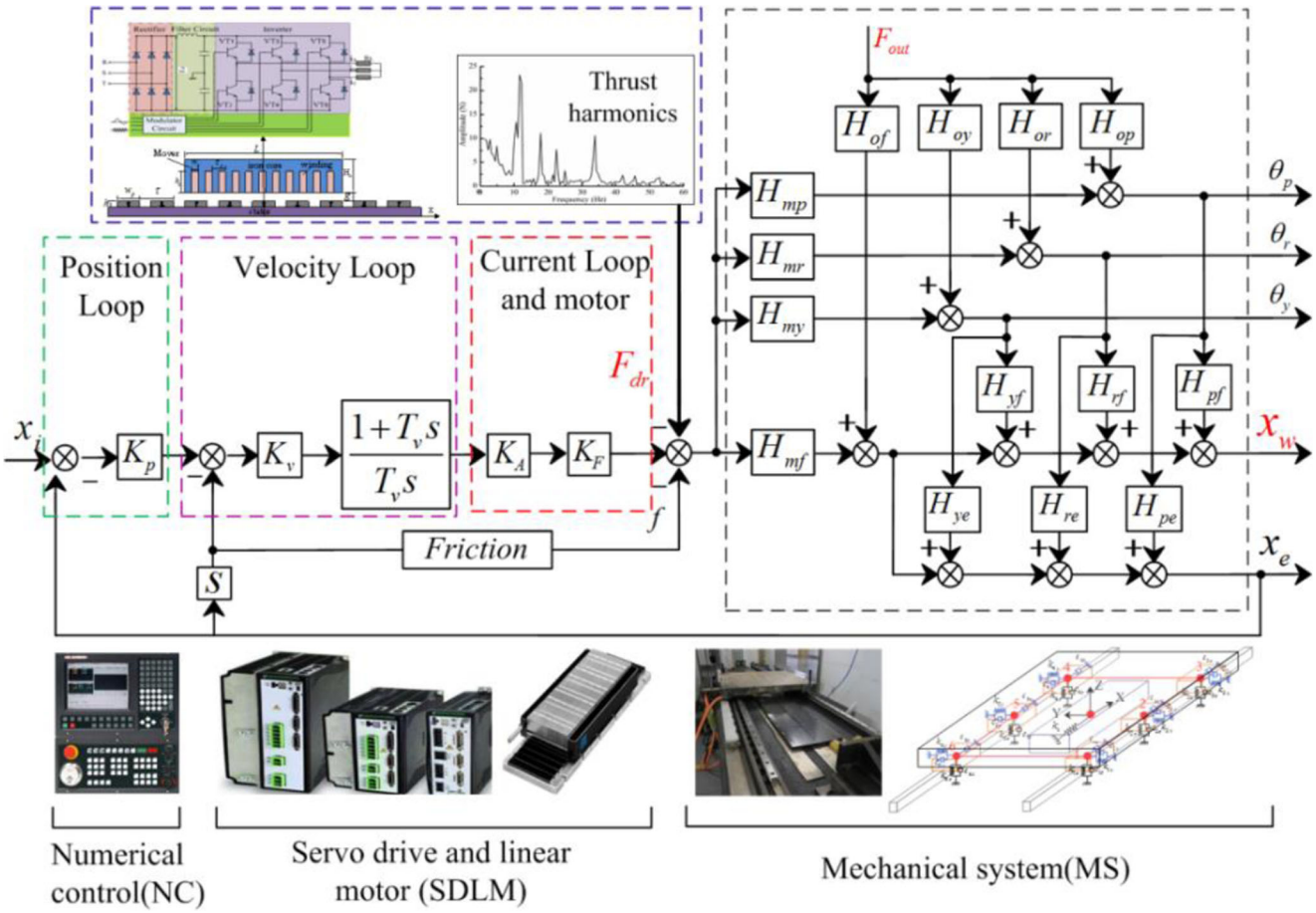

Fig. 10 The electromechanical integrated model of the direct-driven feed system

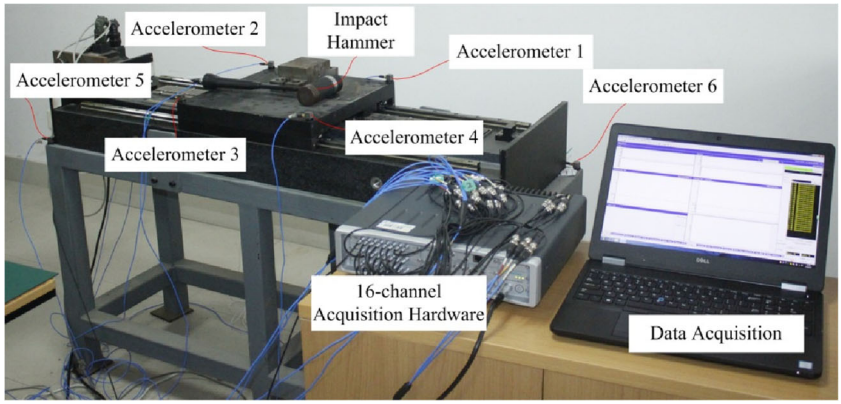

Fig. 11 The test of the mechanical modal

where θ_p, θ_r, and θ_y are the displacement of the worktable in feed direction and angle displacements of rotational vibrations, respectively. F_{motor} and F_{out} are the motor thrust and outside disturbance, respectively. H_{mf}, H_{mp}, H_{mr}, and H_{my} are the transfer functions between the motor thrust and the output of the worktable. H_{of}, H_{op}, H_{or}, and H_{oy} are the transfer functions between the outside disturbance and the output of the worktable. H_{pf}, H_{rf}, and H_{yf} are the conversion functions between the displacement of the worktable and the rotational vibrations. H_{pe}, H_{re}, and H_{ye} are the conversion functions between the displacement of reading head of the linear encoder and the rotational vibrations of the worktable.

Based on the mechanical structure and dynamic model, the transfer functions in Eq. (18) and Eq. (19) can be given by

$$\begin{cases} H_{mf} = \dfrac{1}{ms^2} \\ H_{mp} = \dfrac{M_{mp}}{J_y s^2 + c_{\theta y} s + k_{\theta y}} = \dfrac{M_{mp}}{s^2 + 2\xi_p \omega_p s + \omega_p^2} \\ H_{mr} = \dfrac{M_{mr}}{J_x s^2 + c_{\theta x} s + k_{\theta x}} = \dfrac{M_{mr}}{s^2 + 2\xi_r \omega_r s + \omega_r^2} \\ H_{my} = \dfrac{M_{my}}{J_z s^2 + c_{\theta z} s + k_{\theta z}} = \dfrac{M_{my}}{s^2 + 2\xi_y \omega_y s + \omega_y^2} \end{cases} \tag{20}$$

$$\begin{cases} H_{of} = \dfrac{M_{of}}{ms^2} \\ H_{op} = \dfrac{M_{op}}{J_y s^2 + c_{\theta y} s + k_{\theta y}} = \dfrac{M_{op}}{s^2 + 2\xi_p \omega_p s + \omega_p^2} \\ H_{or} = \dfrac{M_{or}}{J_x s^2{}_r + c_{\theta x} s + k_{\theta x}} = \dfrac{M_{or}}{s^2 + 2\xi_r \omega_r s + \omega_r^2} \\ H_{oy} = \dfrac{M_{oy}}{J_z s^2 + c_{\theta z} s + k_{\theta z}} = \dfrac{M_{oy}}{s^2 + 2\xi_y \omega_y s + \omega_y^2} \end{cases} \tag{21}$$

Table 1 The main parameters of the direct-driven experiment table

Name	Value
Position travel (mm)	600
Maximum velocity (m/min)	30
Maximum acceleration (m/s/s)	15
Mass of the mover and worktable (kg)	44
Cooling	Air cooling
Material of machine bed	The marble
Proportional gain of position controller (1/s)	35
Proportional gain of speed controller (A s/m)	552
Integral time constant of speed controller (s)	0.01
Force constant (N/A)	170
Load (kg)	15
The length of the worktable (mm)	400
The width of the worktable (mm)	400
The distance between two guide rails (mm)	320
The rotational inertia of mechanical system around x-axis Jx (kg m^2)	0.59
The rotational inertia of mechanical system around y-axis Jy (kg m^2)	0.59
The rotational inertia of mechanical system around z-axis Jz (kg m^2)	1.18
The distance between two blocks(mm)	380
The vertical distance between the center of block and mechanical coordinate origin h_b/mm	40
The vertical distance between the center of mover and mechanical coordinate origin h_m/mm	35
The distance between the center of mover and mechanical coordinate origin in y direction/mm	58

Table 2 The mechanical vibration modal of the feed system

Order number	Natural frequency (Hz)	Damping ratio	Mode
1	141.22	0.0119	Roll vibration
2	350.314	0.0135	Vibration in Z direction
3	778.589	0.0175	Yaw vibration
4	817.024	0.0096	Vibration in Y direction
5	884.905	0.0070	Pitch vibration

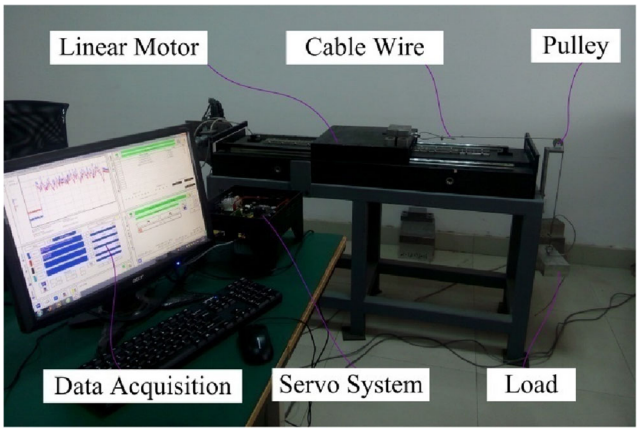

Fig. 12 The test of the displacement command and output

$$\begin{cases} H_{pf} = S_{pf} \\ H_{rf} = S_{rf} \\ H_{yf} = S_{yf} \end{cases} \begin{cases} H_{pe} = S_{pe} \\ H_{re} = S_{re} \\ H_{ye} = S_{ye} \end{cases} \tag{22}$$

where M_{mp}, M_{mr}, and M_{my} represent the equivalent coefficients of motor thrust in three rotational directions. M_o represents the equivalent coefficient of other disturbances in the feed direction. M_{op}, M_{or}, and M_{oy} represent the equivalent coefficients of other disturbances in three rotational directions. ω_p, ω_r, and ω_y are the natural frequencies of the pitch, roll, and yaw, respectively. ξ_p, ξ_r, and ξ_y are the damping ratio of the pitch, roll, and yaw, respectively. S_{pf}, S_{yf}, and S_{rf} are the corrected coefficients between displacement fluctuation and mechanical rotational vibrations. S_{pe}, S_{ye}, and S_{re} are the corrected coefficients between feedback signal and mechanical rotational vibrations.

5 Electromechanical integrated model

Based on the above analysis and electromechanical analytical model in Fig. 2, the nonlinear characteristics of the drive circuit and PMLSM can be expressed as the motor thrust harmonics which are introduced into the model as the interferences. The bandwidth of the current loop is much wider than that of the speed loop and position loop. So the current control loop is initially regarded as ideal for the further considerations [25]. The current loop is equivalent to the proportional gain. The mechanical system is introduced by Eqs. (18) and (19). The friction, which uses the Stribeck model, is added to the system through identifying. Other assumptions are as follows.

1. The process of interpolation, deceleration in the NC is not considered.
2. The system is assumed continuous.
3. The small delay links are ignored.
4. The feed gain of the feedback system is set as 1.

Finally, the electromechanical integrated model of the direct-driven feed system is established as shown in Fig. 10.

In Fig. 10, there are three inputs which are the position command, thrust harmonics, and outside disturbances. There are five outputs which are the displacement of reading head, displacement of the worktable in feed direction, and rotational vibrations of the worktable in pitch, roll, and yaw directions.

Based on the relationship in Fig. 11, the final output of the worktable can be obtained as

$$\begin{aligned} x_0(t) = {} & x_{0x_i}(t) + x_{0\ F_{\text{motor}}}(t) + x_{0\ F_{\text{out}}}(t) + \theta_y(t)\cdot H_{yf} \\ & + \theta_p(t)\cdot H_{pf} + \theta_r(t)\cdot H_{rf} \end{aligned} \tag{23}$$

where $x_{0xi}(t)$ represents the output produced by the command, $x_{0F\text{motor}}(t)$ represents the output produced by thrust harmonics. $x_{0F\text{out}}(t)$ represents the output produced by outside disturbances.

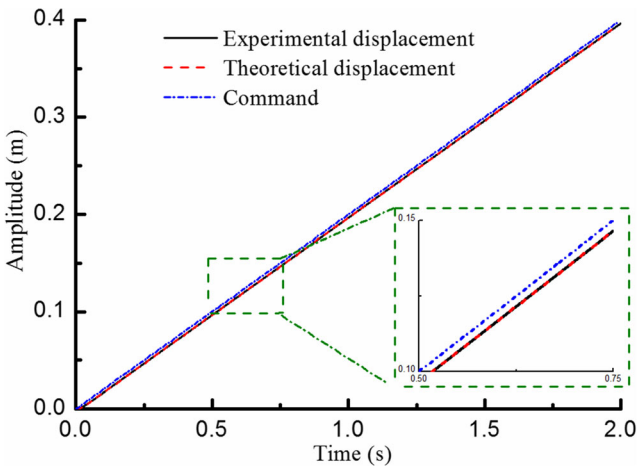

Fig. 13 Comparison of the displacements

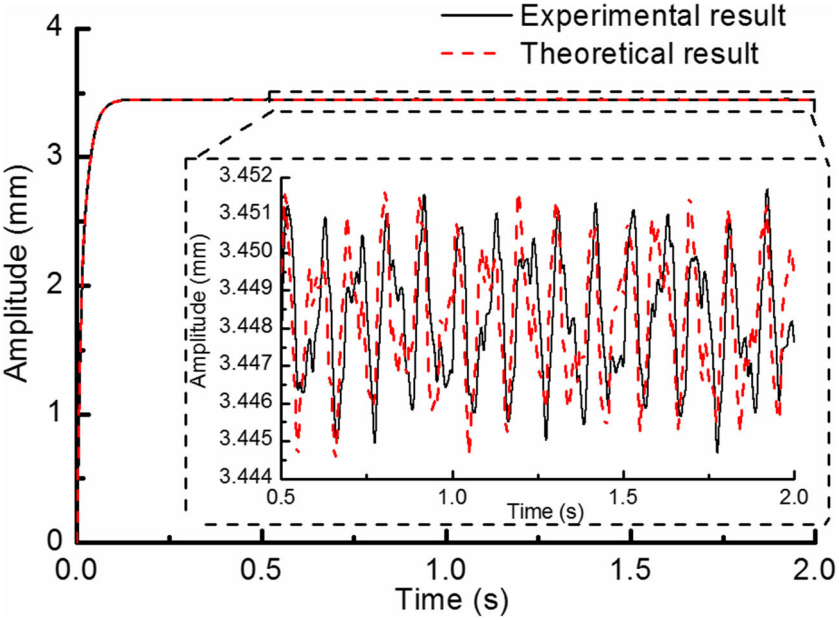

Fig. 14 The deviations between the actual and theoretical displacement and the command

6 Experiments

In order to verify the model, experiments are carried out on a single-axis direct-driven feed system as shown in Fig. 11. The PMLSM (MTPTEK2014-600A) is iron-core permanent magnet synchronous motors, with a mobile coil made by small copper coils wrapped around a laminated ferromagnetic core. The PMLSM stage can be operated by means of pulse commands or velocity commands through the control mode setting of the servo driver. The linear encoder with 0.1-μm resolution is used to measure the position of the worktable. The continuous force of PMLSM is 235 N, and peak force is 600 N. The main parameters of the experiment table are shown in Table 1.

At first, the mechanical parameters are identified by the time domain acquisition module of LMS with a sampling frequency of 1 kHz, which is shown in Fig. 11. The main results are listed in Table 2.

Substituting the results in Table 1 and Table 2 into Eq. (20) and Eq. (21), the transfer functions in Eq. (18) and Eq. (19) can be obtained. What is more, based on the measured motor thrust under different feed speeds, the friction force of the *X*-axis can be fitted by using the Stribeck model, which is shown in Eq. (24).

$$f = 17.89 + (21.83-17.89)e^{-(v/0.01055)^2} + 21.15v \qquad (24)$$

The displacement command and output are collected by the servo system with the sampling frequency of 1 kHz, which is shown in Fig. 12. In the test, all the advanced control methods, such as velocity and acceleration feedforward, are disabled. The speed is 12 m/min. Because the experimental bed cannot

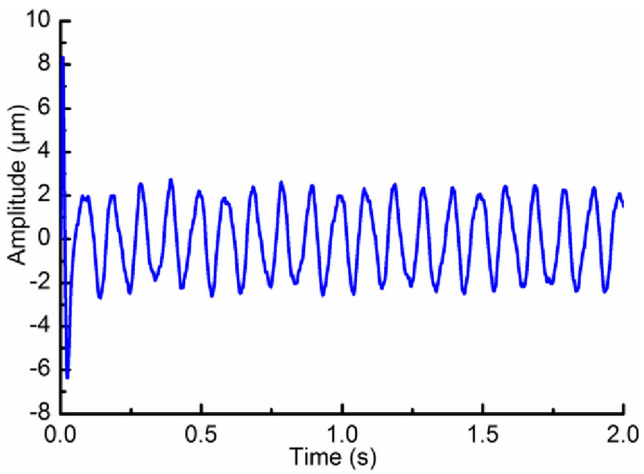

Fig. 15 The deviation of displacement between the actual and theoretical results without following error

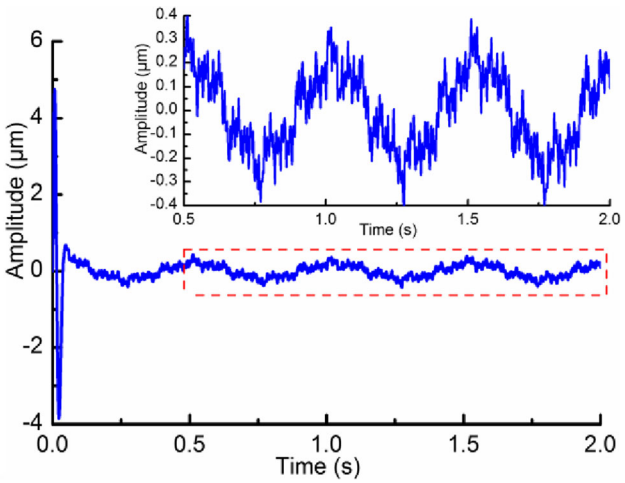

Fig. 16 The deviation of displacement between the actual and theoretical results without following error (considering phase lag)

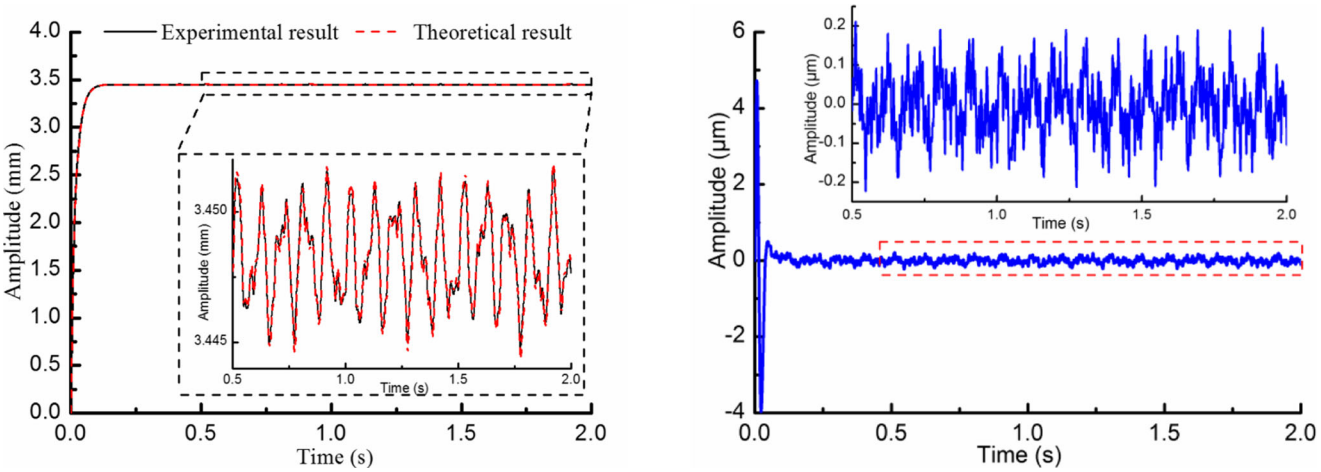

a)following error b) transient error and displacement fluctuation

Fig. 17 The deviation of displacement between the actual and theoretical results without phase lag and geometric error. **a** Following error. **b** Transient error and displacement fluctuation

add the outside disturbances, only the thrust harmonics are considered.

Because of the simple structure of the experimental table, the rotational vibrations of the worktable can be neglected. What is more, the reading head of the linear encoder is mounted in the middle of the worktable. The displacement of the linear encoder is approximately equal to that of the worktable. Therefore, the displacement of the worktable is used as the evaluation index to verify the validity of the theoretical model.

In order to reduce the motion error caused by the mutation of the command, the actual NC command collected by the servo system is taken as the input of the model to calculate the displacement output. The motor thrust calculated by the above theoretical analysis is introduced into the electromechanical integrated model which is shown in Fig. 10. The theoretical displacement can be obtained and then compared with the command and the actual displacement as shown in Fig. 13.

The deviations between the actual and theoretical displacement and the command can be obtained as in Fig. 14.

It can be obtained from Fig. 14 that the deviation of the following error between the actual result and theoretical calculation is about 0.5 μm, which is 0.015% of the actual following error. In order to compare the results of the transient error and displacement fluctuation, the steady-state following error is removed from the displacement. Then the deviation of the motion error between the actual result and theoretical calculation is obtained as shown in Fig. 15.

It can be seen from Fig. 15 that the deviation of transient overshoot error is 8.3 μm and the deviation of displacement fluctuation is 2 μm which is about 55% of the actual fluctuation. It is because that the phase lags of the different thrust harmonics are not considered in the theoretical calculation, which can be revised using the experimental results. Considering the phase lag of each thrust harmonics, the deviation of displacement between the actual and theoretical results without following error can be obtained as shown in Fig. 16.

It can be seen from Fig. 16 that the deviation of the transient overshoot reduces to 4.8 μm and deviation of the displacement fluctuation reduces to 0.4 μm, which is 10.96% of the actual one. However, it can be found that there is obvious harmonics component with frequency of 2 Hz in the deviation, which is considered to be produced by the geometric error of the guide way. The deviation between the actual and theoretical results without geometric error can be obtained in Fig. 17.

It can be seen from Fig. 17 that the deviation of the displacement fluctuation reduces to 0.18 μm, which is 4.93% of the actual one. Validity and reliability of the model and analysis in this paper are proved.

It can be obtained from the above analysis that the proposed integrated model can accurately represent the effects of the NC command, the thrust fluctuations caused by the nonlinearity of servo system, and the mechanical vibration with different modals on the dynamic precision of the direct-driven feed system. The effects of the geometric error and other factors on the dynamic precision are not reflected in the model. However, they can be modified and supplemented by other theoretical analysis.

7 Conclusions

The dynamic characteristics and precision of the direct-driven feed system is codetermined by the characteristics of the servo drive, PMLSM, mechanical system, and their interactions

without considering the cutting process. In this paper, oriented to the dynamic precision, the dynamic characteristics of the drive circuit, PMLSM, control loops, and mechanical system are analyzed systematically and comprehensively. An electromechanical integrated model is established for the direct-driven feed system. The results show that the deviation of the following error between the experiment and calculation is 0.5 μm, which is 0.0015% of the actual error. The deviation of the transient overshoot error between the experiment and calculation is 4.8 μm. The deviation of the displacement fluctuation between the experiment and calculation is 0.18 μm, which is 4.93% of the actual one. The integrated model can accurately represent the characteristics and dynamic precision of the direct-driven feed system, which produces a theoretical foundation for the further research about the electromechanical coupling phenomenon and control compensation.

Funding information This work is financially supported by the key project of the National Natural Science Funds (grant no. 51235009).

References

1. Pritschow G, Philipp W (1990) Direct drives for high-dynamic machine tool axes. Ann CIRP 39(1):413–416
2. Altintas Y, Verl A, Brecher C, Uriarte L, Pritschow G (2011) Machine tool feed drives. CIRP Ann Manuf Technol 60(2):779–796
3. Villegas FJ, Hecker RL, Pena ME, Vicente DA, Flores GM (2014) Modeling of a linear motor feed drive including pre-rolling friction and a periodic cogging and ripple. Int J Adv Manuf Technol 73(1):267–277
4. Tavana NR, Shoulaie A (2011) Pole-shape optimization of permanent magnet linear synchronous motor for reduction of thrust ripple. Energy Convers Manag 52(1):349–354
5. Chang J, Kang DH, Viorel I (2007) Transverse flux reluctance linear motor's analytical model based on finite element method analysis results. IEEE Trans Magn 43(4):1201–1204
6. Yang XJ, Lu D, Ma CF, Zhang J, Zhao WH (2017) Analysis on the multi-dimensional spectrum of thrust force for the linear motor feed drive system in machine tools. Mech Syst Signal Process 82:68–79
7. Zhao SW, Cheung NC, Gan WC (2008) An effective modeling and control strategy for linear switched reluctance motors. Proc Inst Mech Eng C J Mech Eng Sci 222(11):2111–2121
8. Zeng LZ, Chen XD, Li X, Jiang W, Luo X (2015) A thrust force analysis method for permanent magnet linear motor using Schwarz-christoffel mapping and considering slotting effect, end effect and magnet shape. IEEE Trans Magn 51(9):609–617
9. Hor PJ, Zhu ZQ, Howe D (1998) Minimization of cogging force in a linear permanent magnet motor. IEEE Trans Magn 34(5):3544–3547
10. Bazghaleh AZ, Naghashan MR, Mahmodimanesh H, Meshkatoddini MR (2010) Effective design parameters on the end effect in single-sided linear induction motors. World Acad Sci Eng Technol 40:95–100
11. Yang XJ, Lu D, Zhang J, Zhao WH (2015) Dynamic electromechanical coupling resulting from the air-gap fluctuation of the linear motor in machine tools. Int J Mach Tools Manuf 94:100–108
12. Yang XJ, Lu D, Zhang J, Zhao WH (2015) Investigation on the displacement fluctuation of the linear motor feed system considering the linear encoder vibration. Int J Mach Tools Manuf 98:33–40
13. Huang WL, Kuo FC, Chou SC, Yen JY, Tsai IH, Chung TT, Hung CW (2017) High performance and high precision servo control of a single deck dual axis PMLSM stage. Int J Adv Manuf Technol 90(1):865–874
14. Yan MT, Huang KY, Shiu YJ, Chen Y (2007) Disturbance observer and adaptive controller design for a linear motor driven table system. Int J Adv Manuf Technol 35(3):408–415
15. Zhou YF, Song B, Chen XD (2006) Position/force control with a lead compensator for PMLSM drive system. Int J Adv Manuf Technol 30(11):1084–1092
16. Altintas Y, Okwudire CE (2009) Dynamic stiffness enhancement of direct-driven machine tools using sliding mode control with disturbance recovery. CIRP Ann Manuf Technol 58(1):335–338
17. Lee JH, Lee SK (2004) Chucking compliance compensation with a linear motor-driven tool system. Int J Adv Manuf Technol 23(1):102–109
18. Zhang DL, Chen YP, Ai W, Zhou ZD (2007) Precision motion control of permanent magnet linear motors. Int J Adv Manuf Technol 35(3):301–308
19. Elfizy AT, Bone GM, Elbestawi MA (2004) Model-based controller design for machine tool direct feed drives. Int J Mach Tools Manuf 44(5):465–477
20. Yan MT, Cheng TH (2009) High accuracy motion control of linear motor driven wire-EDM machine. Int J Adv Manuf Technol 40(9):918–928
21. Zhu YW, Cho YH (2007) Thrust ripples suppression of permanent magnet linear synchronous motor. IEEE Trans Magn 43(6):2537–2539
22. Kim MS, Chung SC (2005) Chung. A systematic approach to design high-performance feed drive systems. Int J Mach Tools Manuf 45:1421–1435
23. Im H, Yoo HH, Chung J (2011) Dynamic analysis of a BLDC motor with mechanical and electromagnetic interaction due to air gap variation. J Sound Vib 330:1680–1691
24. Neugebauer R, Denkena B, Wegener K (2007) Mechatronic systems for machine tools. CIRP Ann Manuf Technol 56(2):657–686
25. Weck M, Krueger P, Brecher P (2001) Limits for controller settings with electric linear direct drives. Int J Mach Tools Manuf 41(1):65–88
26. Yang XJ, Ma CF, Li Y, Lu D, Zhao WH (2016) A novel evaluation method on the precision of linear motor feed system in high-speed machine tools. Mater Sci Forum 836-837:220–227
27. Youshihiro M, Tomofumi W, Harumitu I (1987) Waveform distortion and correction circuit for PWM inverters with switching lagtimes. IEEE Trans Ind Appl IA23(5):881–886
28. Arahal MR, Barrero F, Ortega MG, Martin C (2016) Harmonics analysis of direct digital control of voltage inverters. Math Comput Simul 130:155–166
29. Subsingha W (2016) A comparative study of sinusoidal PWM and third harmonics injected PWM reference signal on five level diode clamp inverter. Energy Procedia 89:137–148
30. Wang XH, Li QF, Wang SH (2003) Analytical calculation of no-load air-gap magnetic field and back electromotive force in brushless dc motor. Proc CSEE 23(3):126–130
31. Yang XJ, Lu D, Zhao WH (2017) Decoupling and effects of the mechanical vibration on the dynamic precision for the direct-driven machine tool. Int J Adv Manuf Technol 9:1–16